OPEN

Correspondence and
requests for materials
should be addressed to
M.A.N. (mnoginov@
nsu.edu)

Angular distribution of emission from hyperbolic metamaterials

Lei Gu[1], J. E. Livenere[1], G. Zhu[1], T. U. Tumkur[1], H. Hu[2], C. L. Cortes[2], Z. Jacob[2], S. M. Prokes[3]
& M. A. Noginov[1]

[1]Center for Materials Research, Norfolk State University, Norfolk, VA, 23504, USA, [2]Department of Electrical and Computer
Engineering, University of Alberta, Edmonton, AB T6G 2V4, Canada, [3]Electronic Science and Technology Division, Naval Research
Lab, Washington DC, 20375, USA.

We have studied angular distribution of emission of dye molecules deposited on lamellar metal/dielectric
and Si/Ag nanowire based metamaterials with hyperbolic dispersion. In agreement with the theoretical
prediction, the emission pattern of dye on top of lamellar metamaterial is similar to that on top of metal. At
the same time, the effective medium model predicts the emission patterns of the nanowire array and the dye
film deposited on glass to be nearly identical to each other. This is not the case of our experiment. We
tentatively explain the nearly Lambertian ($\propto \cos\theta$) angular distribution of emission of the nanowire based
sample by a surface roughness.

Metamaterials are engineered composite materials consisting of subwavelength units (meta-atoms), which have rationally designed nanostructure, composition and mutual orientation[1,2]. Metamaterials have unique electromagnetic properties, which cannot be found in nature or traditional synthetic materials. Many unparalleled characteristics and breakthrough applications of metamaterials, such as negative index of refraction[3–6], sub-diffraction imaging[7–10], and invisibility cloaking[11,12], have been predicted theoretically and demonstrated experimentally. Metamaterials with hyperbolic dispersion, in which dielectric permittivity components in orthogonal directions have different signs[13–16], possess a broadband singularity in the density of photonic states and can propagate waves with nearly infinitely large wavevectors[17]. They have been shown to control a variety of quantum and classical phenomena, including but not limited to spontaneous emission[17–23] and scattering[24,25].

Inside the volume of a hyperbolic metamaterial, scattered or emitted light propagates in form of beams or cones of light[17]. Because of high emission directionality, combined with high spontaneous emission rate and large quantum yield, hyperbolic metamaterials were proposed to be used as efficient single photon sources in quantum optics applications[17]. At the same time, the angular distribution of emission in far field of hyperbolic metamaterials is much less researched.

Two morphologies most commonly used in the design of hyperbolic metamaterials are metal/dielectric (or semiconductor) lamellar structures[9,15,16] and arrays of parallel metallic nanowires[26–28]. In this Letter, the angular emission diagram of dye molecules in both types of hyperbolic metamaterials is studied both experimentally and theoretically.

Results

Angular distribution of emission on top of lamellar metal-dielectric metamaterials. In the first set of experiments, we have fabricated lamellar metal-dielectric metamaterials with hyperbolic dispersion and spin coated on them thin films of polymethyl methacrylate (PMMA) doped with rhodamine 6G (R6G) laser dye. We have pumped the samples with laser light and studied angular distribution of polarised spontaneous emission. Glass substrates and silver films coated with similar R6G:PMMA films were used as control samples. The details of sample preparation and angular emission measurements are described in Methods. The schematics of the experimental setup is shown in Fig. 1a. The angular distribution of the dye emission on top of multilayer metamaterials (with Ag as outmost layer and MgF$_2$ as outmost layer), silver film and glass slide are shown in Fig. 2.

The results of the measurements can be summarized as follows:

(i) Angular dye emission diagrams in both hyperbolic metamaterials and silver are qualitatively similar to each other (Fig. 2, panels a–c).
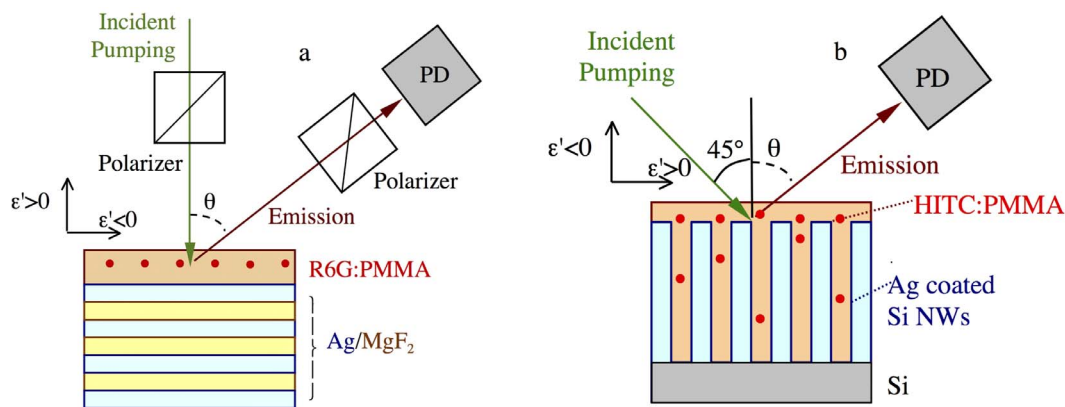
Figure 1 | Experimental setup. Angular measurement of dye emission intensity on top of (a) lamellar Ag/MgF$_2$ metamaterial and (b) Si/Ag nanowire based metamaterial.

In these samples:

(ii) Horizontally polarized emission (p-polarization) has pronounced maximum close to the normal direction, $\theta=0°$. It steadily decreases as angles increase toward 90°.

(iii) Vertically polarized (s-polarized) emission has pronounced shoulders extending down to ~70°.

(iv) In our measurements, the same polarization of the pumping light corresponded to the same pumping intensity. Therefore, the emission intensities (in the polarization conserving and cross polarized channels), which were measured at the same pumping polarization, could be compared against each other. We have found that at vertically polarized pumping, the emission is stronger in the polarization conserving channel (vertically or s-polarized emission) than in the crossed polarized channel (horizontally or p-polarized emission). At the same time, at horizontally polarized pumping, the emission in the polarization conserving channel (p-polarization) was stronger than that in the cross-polarized channel (s-polarization) at $\theta<40°\pm10°$. The p-polarized emission intensity became smaller than the s-polarized emission intensity at larger detection angles.

(v) Angular distribution of dye emission on top of glass is significantly different from that on top of multilayered metamaterials and silver (compare panel d with panels a–c in Fig. 2). It has relatively small signal at normal direction and pronounced maxima at $\theta=55°\pm10°$, Fig. 2d.

(vi) In the dye-doped polymeric film deposited on glass, at both vertically polarized pumping and horizontally polarized pumping, the emission in the polarization conserving channel was stronger than the one in the cross-polarized channel at $\theta\geq40°$. At smaller detection angles, both emission intensities were approximately the same, Fig. 2d.

The latter suggests that the state of polarization and the intensity of polarized emission of dye molecules can be controlled by merely
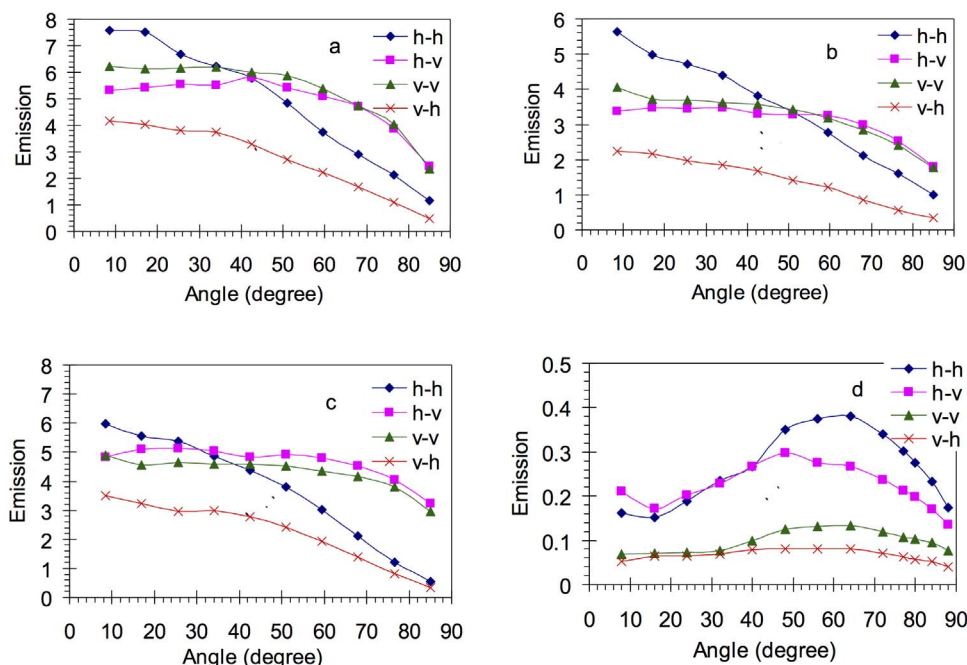

Figure 2 | Angular distribution of emission of R6G dye molecules deposited on top of multilayered metamaterial with Ag as outmost layer (a), multilayered metamaterial with MgF$_2$ as outmost layer (b), 200 nm Ag film (c), and glass (d). Notations "v-v", "v-h", etc. designate vertically or horizontally polarized pumping (first letter) and emission (second letter).

changing the polarization of the pumping beam. In fact, linearly polarized pumping preferentially excites a subset of dye molecules whose dipoles are oriented along the electric field vector, determining the angular distribution and the polarization distribution of spontaneous emission, which are no longer isotropic. The detailed study of this phenomenon is the subject of the future research.

Angular distribution of emission on top of nanowire based metamaterial. In the following, we briefly outline the experimental results of Ref. 29, which will be compared to the theoretical predictions in Discussion. The arrays of aligned silicon nanowires have been fabricated and coated by atomic layer deposition (ALD) of silver[29]. The samples were shown to have hyperbolic dispersion in the most part of visible and near infrared spectrum[29]. The PMMA polymer doped with hexamethylindotrycarbocyanine iodide (HITC) laser dye was deposited on top of the metamaterial. Thermally deposited and ALD silver films coated with the same dye doped polymer were used as control samples. Sample fabrication and measurements of angular emission distribution are described in Methods and Ref. 29. The schematics of the experiment is shown in Fig. 1b.

The measurement results[29] are summarized in Fig. 3. One can see that the angular emission distributions in the Si/Ag nanowire array and ALD silver film are very close to Lambertian, $\sim\cos(\theta)$. At the same time, the angular distribution of spontaneous emission of dye on top of a much smoother (>5 nm roughness) thermally deposited Ag is noticeably broader[29]. To no surprise, it is reasonably close to that observed in R6G doped films deposited on silver, as discussed above, if the average is made over different polarizations of pumping and emission (compare circles and squares in Fig. 4a).

Discussion

Comparison of experimental and theoretical results. In our theoretical study, we have calculated the far-field radiation patterns for both multilayer and nanowire based metamaterial structures. The dyadic Green function formalism was used to model the emission of a dipole placed above the structure. The asymptotic far-field behavior ($R\cdot\omega/c\gg1$) is obtained by using the method of stationary phase with the typical Green function expression above a planar system. The result for the far-field power is given by[30,31]

$$<P_{ff}(\theta)> = \mu_\perp^2 p_\perp^{(p)}(\theta) + \frac{1}{2}\mu_{||}^2 p_{||}^{(p)}(\theta) + \frac{1}{2}\mu_{||}^2(\theta) p_{||}^{(s)}(\theta),$$

where $<>$ denotes dipole averaging over azimuthal angle ϕ due to the isotropic orientation of the dipoles parallel to the interface. To obtain the randomly-oriented dipole case, we also average over the inclination angle, so that the parallel and perpendicular dipole moments ($\mu_{||}$, $\mu_\perp$) are replaced by $<\mu_{||}^2> = 2/3, <\mu_\perp^2> = 1/3$. The far-field power coefficients $p_\perp^{(p)}(\theta), p_{||}^{(p)}(\theta), p_{||}^{(s)}(\theta)$ represent the p-polarized and s-polarized contributions from the perpendicular and parallel dipole components, containing both incident and reflected wave contributions.

We have calculated the angular emission distribution diagrams using the effective medium theory for a dielectric (glass), metal, multilayer metamaterial and nanowire metamaterial substrates, Fig. 4. In the effective medium approximation, at the laser wavelengths used in our experiments, the multilayer structure behaves like a hyperbolic metamaterial with $Re\{\varepsilon_\perp\}>0, Re\{\varepsilon_{||}\}<0$, while the nanowire structure behaves like a hyperbolic metamaterial with $Re\{\varepsilon_\perp\}<0, Re\{\varepsilon_{||}\}>0$.

In agreement with Ref. 32, our model predicts that (1) the dye on top of a lamellar metamaterial ($Re\{\varepsilon_\perp\}>0, Re\{\varepsilon_{||}\}<0$) has nearly the same angular emission behavior as the dye on top of a metallic film, and (2) the angular distribution diagram of dye on top of a nanowire based metamaterial ($Re\{\varepsilon_\perp\}<0, Re\{\varepsilon_{||}\}>0$) should be similar to that on top of a dielectric. The first theoretical prediction is in agreement with our experiment, and the calculated and experimental curves for metal and lamellar metamaterial have closely matching shapes, Fig. 4a.

At the same time, the second prediction does not agree with the experiment so well. Although the experimental and the calculated angular emission diagrams for dye molecules on top of glass have the same characteristic shapes, the experimental and the theoretical curves for the nanowire based metamaterial are strongly different from each other (Fig. 4b). This disagreement can probably be explained by the fact that Si nanowires have slightly different heights (± 200 nm), making the sample's surface rough, which leads to the Lambertian ($\propto\cos\theta$) angular distribution of emission intensity[33] (Fig. 3). Surface roughness can probably also explain the Lambertian distribution of emission on top of ALD silver film[34], although the roughness of the ALD silver is smaller than that of the Si/Ag nanowire array.

To summarize, we have studied angular distribution of emission of dye molecules deposited on lamellar metal/dielectric ($Re\{\varepsilon_\perp\}>0, Re\{\varepsilon_{||}\}<0$) and nanowire based ($Re\{\varepsilon_\perp\}<0, Re\{\varepsilon_{||}\}>0$) metamaterials with hyperbolic dispersion. In good agreement with the theoretical prediction, the emission pattern of dye on top of lamellar metamaterial is similar to that on top of metal. At the same time, the effective medium model predicts the angular distribution of emission from a nanowire array to be similar to that from the dye film deposited on glass. This is not the case of our experiment. Although the calculated and the experimental emission patterns of dye molecules deposited on glass have qualitatively similar shapes, the model and the experiment strongly disagree in the case of the nanowire based array. We tentatively explain the nearly Lambertian ($\propto\cos\theta$) angular distribution of emission intensity in the nanowire based sample by a substantial surface roughness. More theoretical and experimental studies of the emission's polarization state is the subject of the future work.
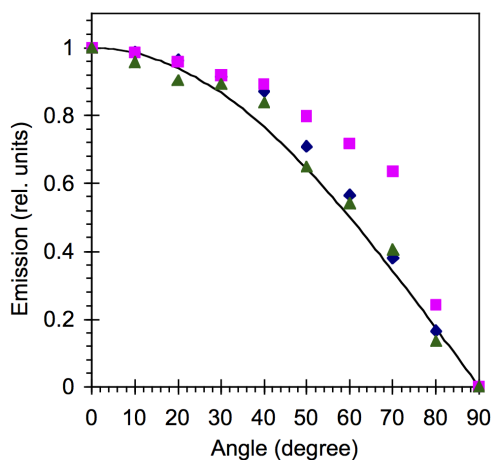
Methods

Figure 3 | Angular distributions of unpolarized emission of HITC dye molecules on top of Si/Ag nanowire array (diamonds), ALD silver film (triangles) and silver film deposited via thermal vapor deposition (squares). Solid line: $\cos(\theta)$. Adopted from Ref. 29.
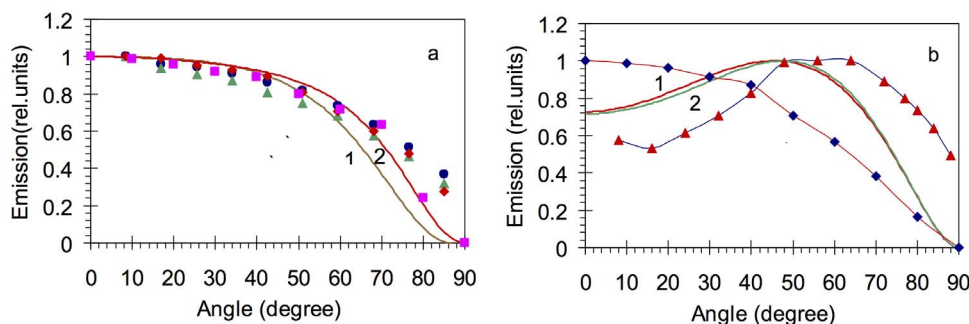
Figure 4 | (a) Theoretical modeling: Angular emission distribution calculated for randomly oriented emitting dipoles positioned 20 nm above a metal ($\varepsilon=-5+0.01i$) (trace 1) and effective medium metamaterial ($\varepsilon_{||}=-5+0.01i$ and $\varepsilon_{\perp}=5+0.01i$) (trace 2). Experiment: Angular distribution of R6G emission on top of 200 nm Ag film (circles), multilayered metamaterial with Ag as outmost layer (diamonds), and metamaterial with MgF$_2$ as outmost layer (triangles). Same for HITC emission on top of Ag film (squares). Circles, squares and triangles depict the data from Figs. 2 a–c averaged over different pumping and emission polarizations. Squares – same as in Fig. 3. (b) Theoretical modeling: Angular emission distribution for randomly oriented emitting dipoles positioned 20 nm above a glass ($\varepsilon=5+0.01i$) (trace 1) and effective medium metamateial ($\varepsilon_{||}=5+0.01i$ and $\varepsilon_{\perp}=-5+0.01i$) (trace 2). Experiment: Angular distribution of R6G emission on top of glass (triangles) and nanowire based metamaterial (diamonds). Triangles depict the data from Fig. 2d averaged over different pumping and emission polarizations. Diamonds – same as in Fig. 3. All curves are normalized to unity at maximum.

dispersion (negative dielectric permittivity Re$\{\varepsilon_{||}\}$ in the direction parallel to the metamaterial's surface and positive dielectric permittivity Re$\{\varepsilon_{\perp}\}$ in the direction perpendicular to the metamaterial's surface) in the spectral range of interest, $\lambda > 360$ nm[22].

Thin films of polymethyl methacrylate (PMMA) doped with rhodamine 6G (R6G) laser dye were spin coated on top of metamaterial substrates. The dye concentration in PMMA was equal to 10 g/l (0.033 M). Similar dye-doped PMMA films deposited on glass and on ~200 nm Ag films were used as control samples. At the wavlength of R6G emission, ~575 nm, the values of effective dielectric permittivities of the metamaterial in the directions parallel || and perpendicular ⊥ to the sample's surface were equal to Re$\{\varepsilon_{||}\}= -4.6$, Im$\{\varepsilon_{||}\}= 0.16$, Re$\{\varepsilon_{\perp}\}=3.5$, and Im$\{\varepsilon_{\perp}\}=0.01$[35].

Nanowire based metamaterial. The aligned silicon nanowire arrays (150 nm nanowire diameter, 250 nm center to center distance, ~30 μm length) were fabricated by using chemical etching and coated by atomic layer deposition (ALD) of Ag (with the thickness of 38 nm)[29]. The real values of effective dielectric permittivity in this material (at $\lambda=900$ nm) are equal to Re$\{\varepsilon_{||}\}=2.4$ and Re$\{\varepsilon_{\perp}\}=-12$[29].

The PMMA polymer doped with HITC laser dye (in concentration 0.04 M) was deposited on top of the metamaterial, where it penetrated between the wires. Dye-doped PMMA films (~80 nm) deposited onto ALD Ag film and thermally deposited Ag film were used as control samples. They had the same concentration of dye molecules per unit area as the metamaterial[29].

Angular emission measurements. *R6G:PMMA on top of lamellar metamaterials and control samples.* The angular emission measurements were performed at excitation of R6G dye molecules with the frequency-doubled Q-switched Nd:YAG laser ($\lambda_{pump} = 532$ nm, $t_{pulse} \approx 12$ ns). The incident light was either horizontally polarized or vertically polarized. The angle of incidence was nearly normal to the sample's surface. The intensity of the vertically polarized (s-polarized) and horizontally polarized (p-polarized) emission in the spectral band centered at 570 nm was measured at a variety of angles ranging from 5° to ±85° (0° is normal to the sample surface and ±90° is parallel to the surface. A long-pass color filter located in front of the detector blocked laser light and transmitted dye emission only, Fig. 1a. In the measurements, we used four different combinations of pumping and emission polarizations: horizontally polarized pumping and horizontally polarized emission (h-h), horizontally polarized pumping and vertically polarized emission (h-v), vertically polarized pumping and horizontally polarized emission (v-h), and vertically polarized pumping and vertically polarized emission (v-v).

HITC:PMMA on top of nanowire based metamaterial and sontrol samples. Dye molecules were excited with ~5 nm pulses of the optical parametric oscillator (OPO) at $\lambda = 750$ nm and 45° incidence angle, Fig. 1b. The (unpolarized) emission distribution diagrams were measured at a variety of angles in the spectral band centered at 815 nm[29].

1. Engheta, N. & Ziolkowski, R. W. *Metamaterials: Physics and Engineering Explorations*. 3–30 (Wiley & Sons, New York, 2006).
2. Noginov, M. A. & Podolskiy, V. A. *Tutorials in Metamaterials*. (Taylor & Fancis, Boca Raton, 2012).
3. Veselago, V. G. The electrodynamics of substances with simultaneously negative values of ε and μ. *Sov. Phys. Usp.* **10**, 509–514 (1968).
4. Pendry, J. B. Negative Refraction Makes a Perfect Lens. *Phys. Rev. Lett.* **85**, 3966–3969 (2000).
5. Shelby, R. A., Smith, D. R. & Schultz, S. Experimental verification of a negative index of refraction. *Science* **292**, 77–79 (2001).
6. Shalaev, V. M. *et al.* Negative index of refraction in optical metamaterials. *Opt. Lett.* **30**, 3356–3358 (2005).
7. Fang, N., Lee, H., Sun, C. & Zhang, X. Sub-Diffraction-Limited optical imaging with a silver superlens. *Science* **308**, 534–537 (2005).
8. Blaikie, R. J. & Melville, D. O. S. Imaging through planar silver lenses in the optical near field. *J. Opt. A: Pure Appl. Opt.* **7**, S176–S183 (2005).
9. Liu, Z., Lee, H., Xiong, Y., Sun, C. & Zhang, X. Far-field optical hyperlens magnifying sub-diffraction-limited objects. *Science* **315**, 1686 (2007).
10. Smolyaninov, I. I., Hung, Y. J. & Davis, C. C. Magnifying superlens in the visible frequency range. *Science* **315**, 1699–1701 (2007).
11. Pendry, J. B., Schurig, D. & Smith, D. R. Controlling electromagnetic fields. *Science* **312**, 1780–1782 (2006).
12. Cai, W., Chettiar, U. K., Kildishev, A. V. & Shalaev, V. M. Optical cloaking with metamaterials. *Nat. Photonics* **1**, 224–227 (2007).
13. Smith, D. R. & Schurig, D. Electromagnetic wave propagation in media with indefinite permittivity and permeability tensors. *Phys. Rev. Lett.* **90**, 077405 (2003).
14. Belov, P. A. *et al.* Strong spatial dispersion in wire media in the very large wavelength limit. *Phys. Rev. B* **67**, 113103 (2003).
15. Jacob, Z., Alekseyev, L. V. & Narimanov, E. E. Optical Hyperlens: Far-field imaging beyond the diffraction limit. *Opt. Express* **14**, 8247–8256 (2006).
16. Salandrino, A. A. & Engheta, N. Far-field subdiffraction optical microscopy using metamaterial crystals: Theory and simulations. *Phys. Rev. B* **74**, 075103 (2006).
17. Jacob, Z., Smolyaninov, I. I. & Narimanov, E. E. Broadband Purcell effect: Radiative decay engineering with metamaterials. *Appl. Phys. Lett.* **100**, 181105 (2012).
18. Poddubny, A. N., Belov, P. A. & Kivshar, Y. S. Spontaneous radiation of a finite-size dipole emitter in hyperbolic media. *Phys. Rev. A* **84**, 023807 (2011).
19. Noginov, M. A. *et al.* Controlling spontaneous emission with metamaterials. *Opt. Lett.* **35**, 1863–1865 (2010).
20. Jacob, Z. *et al.* Engineering photonic density of states using metamaterials. *Appl. Phys. B: Lasers and Optics* **100**, 215–218 (2010).
21. Krishnamoorthy, H. N. S., Jacob, Z., Narimanov, E. E., Kretzschmar, I. & Menon, V. M. Topological Transitions in Metamaterials. *Science* **336**, 205–209 (2012).
22. Tumkur, T. U. *et al.* Control of spontaneous emission in a volume of functionalized hyperbolic metamaterial. *Appl. Phys. Lett.* **99**, 151115 (2011).
23. Kim, J. *et al.* Improving the radiative decay rate for dye molecules with hyperbolic metamaterials. *Opt. Express* **20**, 8100–8116 (2012).
24. Tumkur, T. U. *et al.* Control of reflectance and transmittance in scattering and curvilinear hyperbolic metamaterials. *Appl. Phys. Lett.* **101**, 091105 (2012).
25. Narimanov, E. E., Li, H., Barnakov, Y. A., Tumkur, T. U. & Noginov, M. A. Reduced reflection from roughened hyperbolic metamaterial. *Optics Express* **21**, 14956–14961 (2013).
26. Yao, J. *et al.* Optical negative refraction in bulk metamaterials of nanowires. *Science* **321**, 930 (2008).
27. Dickson, W. *et al.* Dielectric-loaded plasmonic nanoantenna arrays: A metamaterial with tuneable optical properties. *Phys. Review B* **76**, 115411 (2007).
28. Noginov, M. A., Barnakov, Y. A., Zhu, G., Tumkur, T. U., Li, H. & Narimanov, E. E. Bulk photonic metamaterial with hyperbolic dispersion. *Appl. Phys. Lett.* **94**, 151105 (2009).
29. Prokes, S. M. *et al.* Hyperbolic and plasmonic properties of Silicon/Ag aligned nanowire arrays. *Optics Express* **21**, 14962–14974 (2013).

30. Novotny, L. & Hecht, B. *Principles of nano-optics.* (Cambridge University Press, New York, 2006).
31. Mandel, L. & Wolf, E. *Optical Coherence and Quantum Optics.* (Cambridge University Press, New York, 1995).
32. Cortes, C. L., Newman, W., Molesky, S. & Jacob, Z. Quantum nanophotonics using hyperbolic metamaterials. *Journal of Optics*, **14**(6), 063001 (2012).
33. Nieto-Vesperinas, M. Random rough surfaces that produce a Lambertian distribution of radiant intensity. *Opt. Lett.* **7**, 165–167 (1982).
34. Prokes, S. M. *et al.* Spoof-like plasmonic behavior of plasma enhanced atomic layer deposition grown Ag thin films. *Appl. Phys. Lett.* **100**, 053106 (2012).
35. Tumkur, T. U. *et al.* Control of spontaneous emission with functionalized multilayered hyperbolic metamaterials, in Metamaterials: Fundamentals and Applications IV 80930O, Proceedings of SPIE Vol. 8093, SPIE, Bellingham, WA. DOI:10.1117/12.896033 (2011 September 13).

Acknowledgments

Author contributions

L.G., J.E.L. and G.Z. conducted the experiments and performed the data analysis. T.U.T. and S.M.P. fabricated the samples. H.H., C.L.C. and Z.J. conducted theoretical computation. M.A.N. has designed the experiment. L.G. and M.A.N. wrote the manuscript.

Additional information

Competing financial interests: The authors declare no competing financial interests.

How to cite this article: Gu, L. *et al.* Angular distribution of emission from hyperbolic metamaterials. *Sci. Rep.* **4**, 7327; DOI:10.1038/srep07327 (2014).